Hindawi
Shock and Vibration
Volume 2019, Article ID 3707416, 14 pages
https://doi.org/10.1155/2019/3707416

Research Article

Modeling and Analysis of Vehicle Shimmy with Consideration of the Coupling Effects of Vehicle Body

Xiaogao Li,[1,2] **Ning Zhang**,[1] **Xianjian Jin**,[3] **and Nan Chen**[1]

[1]*School of Mechanical Engineering, Southeast University, Nanjing 211189, China*
[2]*School of Mechanical and Electronic Engineering, Jingdezhen Ceramic Institute, Jingdezhen 333403, China*
[3]*School of Mechatronic Engineering and Automation, Shanghai University, Shanghai 200072, China*

Correspondence should be addressed to Nan Chen; nchen@seu.edu.cn

Received 17 November 2018; Revised 7 January 2019; Accepted 6 February 2019; Published 24 March 2019

Academic Editor: Angelo Marcelo Tusset

Based on the Lagrange equation, a 9-degrees-of-freedom shimmy model with consideration of the coupling effects between the motions of vehicle body and the shimmy of front wheels and a 5-degrees-of-freedom shimmy model ignoring these coupling effects for a vehicle with double-wishbone independent front suspensions are presented here to study the problem of vehicle shimmy. According to the eigenvalue loci of system's Jacobian matrix plotted on the complex plane, the Hopf bifurcation characteristics of nonlinear shimmy are studied and the conditions for the generation of limit cycle are analyzed. Numerical calculation and simulation are used to study the dynamic behavior of vehicle shimmy. By comparing the dynamic responses of two different shimmy models, the coupling effects of vehicle body on vehicle shimmy are studied. Finally, the relationship between the amplitude of each DoF and vehicle velocity and the influences of vehicle parameters such as the mass of vehicle body, the longitudinal position of the center of gravity of vehicle body, and the inclination angle of front suspension on shimmy are studied.

1. Introduction

Shimmy phenomenon, which widely exists in vehicles, motorcycle and landing gear of airplane, is a problem of nonlinear dynamics [1–3]. Vehicle shimmy is a sustained oscillation of the steering wheels around the kingpin, combined with the lateral yaw motion caused by the interaction between the tire and the dynamic behavior of steering system. It is closely related to the control stability, ride performance, dynamic property, fuel economic, and safety of the vehicle. Thus, it is still a problem for engineers to eliminate shimmy completely in the design phase of vehicles.

Since De Lavaud [4] published the first paper on wheel shimmy in 1920s, a large number of investigations have been conducted to study the phenomenon of vehicle shimmy in the past decades. Recent research studies indicate that the main factors which affect vehicle shimmy are (a) the dynamic response of tires, (b) the parameters of suspensions and steering system, and (c) the clearance and friction in mechanical structures. Von Schlippe and Dietrich [5] introduced the kinematics theory of pure rolling wheel and the finite contact length stretched string tire model in the early 1940s. Thereafter, more and more scholars focused on the problem of tire dynamics and set up several tire mathematical models for vehicle dynamics analysis. Pacejka et al. [6, 7] did a more comprehensive study on the problem of wheel shimmy, especially on constructing the mathematical model of tire, and developed the famous Magic Formula [8]. Gim and Nikravesh [9] studied the dynamic properties of tire due to pure slips and comprehensive slips and analytically derived the explicit formulations for the tire dynamic properties. Gim's tire model can be used to calculate the forces and moments between the pneumatic tires and the road surface. Guo and Lu [10] established the UniTire model, which is a nonlinear and non-steady-state tire model for vehicle dynamics simulation and control. In recent years, because of the establishment of the above tire model and continuous improvement, great progress has been made in the research on the problem of vehicle shimmy. Takács and Stépan

[11, 12] have made rich achievements in the research of the shimmy problem, involving modeling of tire, modeling of steering system, and modeling of suspension system. Ran et al. [13] studied the effects of the nonlinearities in tire on the stability of vehicle shimmy by the energy flow method. Wei et al. [14] developed a nine-degrees-of-freedom (DoF) dynamic model to study the shimmy of a dual front axle heavy truck. Lu et al. [15–17] performed a comprehensive study on vehicle shimmy in which the clearance in mechanism structure, such as in the steering linkage mechanism, the steering handling mechanism, and the cross shaft type universal joint, is taken into account, and the effect of the roll motion of vehicle body to vehicle shimmy is also considered. With the rapid development of new energy vehicle, the shimmy problem of electric vehicle stimulates the interest of some researchers. For instance, Mi et al. [18] paid more attention to the shimmy problem of electric vehicle with independent suspensions.

Most of the above research studies are based on the assumption that vehicle body is stationary, and the effects of the motions of vehicle body, such as yaw, pitch, roll, and lateral and vertical motion, on the shimmy of front wheels are ignored. But in fact, the shimmy of front wheels around the kingpins will produce the forces acting on the vehicle body, and the motions of the vehicle body certainly affect the shimmy of the front wheels. Therefore, there are coupling effects between the shimmy of the front wheels and the motions of the vehicle body. However, it is still not clear how the motions of vehicle body affect the dynamic behavior of vehicle shimmy. Independent suspensions are widely used in vehicles, and the dynamic model of a vehicle with independent front suspension structure is presented here. Based on the numerical analysis, the coupling effects between vehicle shimmy and the motions of vehicle body are discussed with the time history response and the phase portrait of each DoF of vehicle shimmy. Meanwhile the relationships between the parameters of vehicle body and the shimmy of front wheels are presented here.

The rest of this paper will be organized as follows. Mechanical and mathematical models for vehicle shimmy are established in Section 2. The Hopf bifurcation characteristics of two systems are analyzed in Section 3. Numerical simulation is carried out in Section 4. The influences of parameters related to vehicle body and front suspensions on shimmy are studied in Section 5. Some conclusive remarks are given at the end.

2. Vehicle Shimmy Model

2.1. Mechanical Model of Vehicle Shimmy with Consideration of the Motions of Vehicle Body. The mechanical model of shimmy with consideration of the coupling effects of the motions of vehicle body for a vehicle with double-wishbone independent front suspensions is shown in Figure 1. In line with the law of right-hand coordinate system, the coordinate axes *ox*, *oy*, and *oz* point to the front, the left, and the top of the vehicle, respectively.

To facilitate dynamic analysis and mathematical modeling, the following assumptions are made to establish a dynamics model for vehicle shimmy.

(1) The steering wheel is immobile

(2) The effect of air resistance is neglected

(3) The plane of steering trapezium is parallel to the horizontal plane *xoy*

(4) The vehicle keeps moving at a constant velocity, and without cornering

(5) The effect of the caster angle is considered, while other alignment parameters are neglected

(6) Vehicle structure is bilaterally symmetrical

(7) The central lines of the spring of rear suspension are perpendicular to the horizontal plane, and the vertical height of front and the rear suspensions are the same

(8) The mass other than wheels and vehicle body will not be considered

Parameters related to the structure size of the vehicle are marked on the mechanical model of vehicle shimmy, as shown in Figure 1. In which, W_f and W_r are half of the distances between two connection points where the dampers of the front and rear suspensions connect with the vehicle body, respectively; L_f and L_r are the distances from vehicle body's CoG to the connection line of two connection points where the dampers of front and rear suspensions connect with the vehicle body, respectively; l_a is the horizontal distance of connection points between the vehicle body and suspension arm, suspension spring; l_b is the distance from the intersection point of the kingpin extension line and the ground to the symmetry plane of the wheel; l_c is the horizontal distance between the two ends of the suspension spring; l_d is the arm of force of steering rod acting on kingpin; l_f is the lateral swing arm of front suspension; l_g is the arm of force of steering tie rod acting on pitman arm; l_h is the vertical height between the two ends of suspension spring, namely, the vertical height of front suspension springs and rear suspension springs.

2.2. Lagrange Equation. According to the mechanical model of vehicle shimmy with consideration of the coupling effects of the motions of the vehicle body, its mathematical model can be established. This shimmy model has nine DoFs: $\theta_{1,2}$ are the angles of front wheels swing that revolve around their respective kingpin (namely, the shimmy angles), θ_3 is the angle of pitman arm's swing in steering system, $\varphi_{1,2}$ are the angles of front wheel axes' lateral swing that revolve around their respective lateral swing centers which are parallel to the x axis, $\theta_{r,p,\omega}$ are the roll, pitch, and yaw angle of vehicle body respectively, and z is the displacement of vehicle body along the z axis.

The mathematical model of vehicle shimmy can be established based on the Lagrange equations which are expressed as

$$\frac{d}{dt}\left(\frac{\partial T}{\partial \dot{q}_i}\right) - \frac{\partial T}{\partial q_i} + \frac{\partial U}{\partial q_i} + \frac{\partial D}{\partial \dot{q}_i} = Q_i, \quad i = 1, 2, 3, \ldots, 9. \tag{1}$$

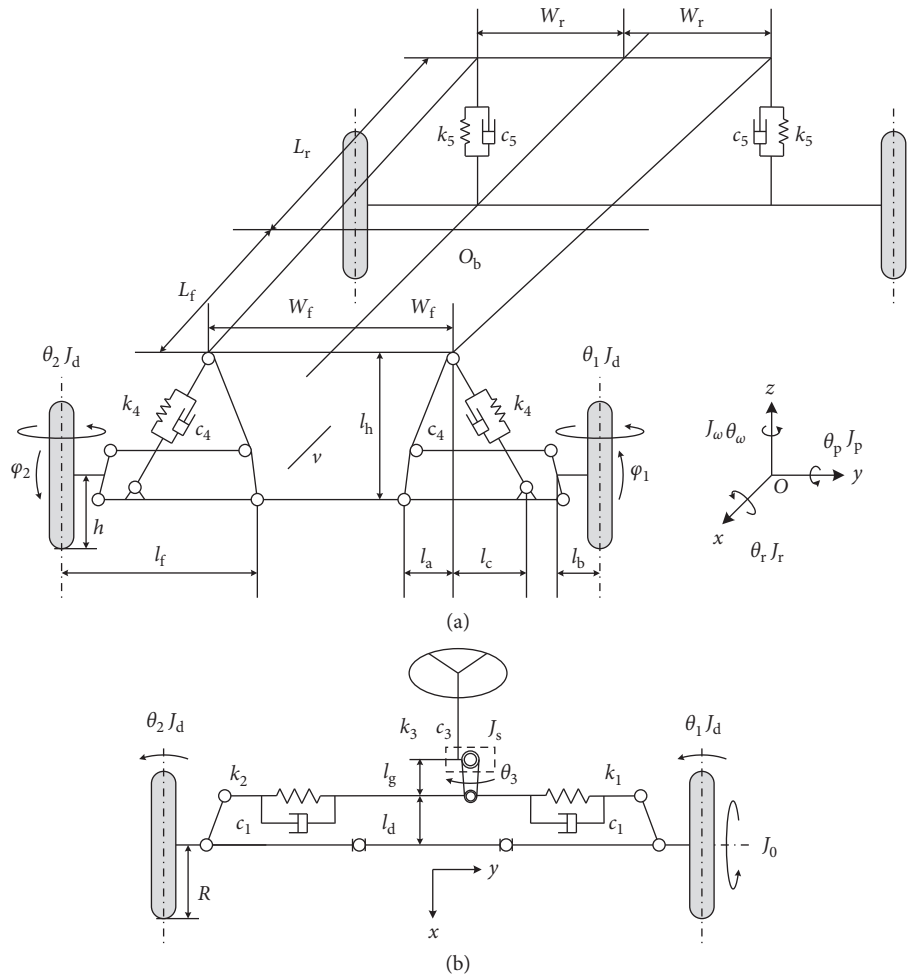

Figure 1: Mechanical model of vehicle shimmy with consideration of vehicle body. (a) Three-dimensional view. (b) Vertical view of steering system.

where T represents the kinetic energy of the system, U represents the potential energy of the system, D represents the dissipative potential function of the system, Q_i represents the generalized force to which each DoF of the system is subjected, and q_i represents the generalized coordinate of the system, which is expressed as $[q_1\ q_2\ \cdots\ q_9] = [\theta_1\ \theta_2\ \theta_3\ \varphi_1\ \varphi_2\ \theta_r\ \theta_p\ \theta_\omega\ z]$.

The kinetic energy of the system can be given by

$$\begin{aligned} T = {} & \frac{1}{2}J_d\dot{\varphi}_1^2 + \frac{1}{2}J_0\left(\frac{v}{R} - \dot{\varphi}_1\theta_1\right)^2 + \frac{1}{2}J_d\left(\dot{\theta}_1 - \dot{\varphi}_1\gamma\right)^2 \\ & + \frac{1}{2}m_\omega\left(v - l_b\dot{\theta}_1\right)^2 + \frac{1}{2}m_\omega\left(l_f\dot{\varphi}_1 - l_b\dot{\theta}_1\gamma\right)^2 + \frac{1}{2}J_d\dot{\varphi}_2^2 \\ & + \frac{1}{2}J_0\left(\frac{v}{R} - \dot{\varphi}_2\theta_2\right)^2 + \frac{1}{2}J_d\left(\dot{\theta}_2 - \dot{\varphi}_2\gamma\right)^2 + \frac{1}{2}m_\omega\left(v - l_b\dot{\theta}_2\right)^2 \\ & + \frac{1}{2}m_\omega\left(l_f\dot{\varphi}_2 - l_b\dot{\theta}_2\gamma\right)^2 + \frac{1}{2}J_3\dot{\theta}_3^2 + \frac{1}{2}m_s v^2 + \frac{1}{2}m_s\dot{z}^2 + \frac{1}{2}J_r\dot{\theta}_r^2 \\ & + \frac{1}{2}J_p\dot{\theta}_p^2 + \frac{1}{2}J_\omega\dot{\theta}_\omega^2, \end{aligned} \tag{2}$$

where J_0 and J_d are the moments of inertia of front wheels around spin axes and diameters, respectively; J_3 is the moment of inertia of the pitman arm; J_r, J_p, and J_ω are the moments of inertia of vehicle body around the x, y, and z axis, respectively; m_w is the mass of wheels, and m_s is the mass of vehicle body; γ is the caster angle of front wheels; R is the rolling radius of tires; and v is the vehicle velocity.

The potential energy of the system is given by

$$\begin{aligned} U = {} & \frac{1}{2}k_1\left(l_d\theta_1 - l_g\theta_3\right)^2 + \frac{1}{2}k_2\left(l_g\theta_3 - l_d\theta_2\right)^2 + \frac{1}{2}k_3\theta_3^2 \\ & + \frac{1}{2}k_4\left(\Delta_{fl}^2 + \Delta_{fr}^2\right) + \frac{1}{2}k_5\left(\Delta_{rl}^2 + \Delta_{rr}^2\right) + \frac{1}{2}k_b\left(l_f\varphi_1 - l_b\theta_1\gamma\right)^2 \\ & + \frac{1}{2}k_b\left(l_f\varphi_2 - l_b\theta_2\gamma\right)^2 + \frac{1}{2}k_y\left(R\varphi_1 - R\theta_1\gamma\right)^2 \\ & + \frac{1}{2}k_y\left(R\varphi_2 - R\theta_2\gamma\right)^2, \end{aligned} \tag{3}$$

where k_1 and k_2 are the stiffness of left and right steering tie rods, respectively; k_3 is the stiffness of pitman arm; k_4 and k_5 are the stiffness of front and rear suspensions, respectively;

k_y is tire lateral stiffness; k_b is tire vertical stiffness; Δ_{fl}, Δ_{fr}, Δ_{rl}, and Δ_{rr} are the deformations of the front-left, front-right, rear-left, and rear-right suspensions, respectively, which are given by equation (8).

The dissipative potential function is given by

$$\begin{aligned} D = {} & \frac{1}{2}c_{\mathrm{e}}\left(\dot{\theta}_1^2 + \dot{\theta}_2^2\right) + \frac{1}{2}c_1\left(l_{\mathrm{d}}\dot{\theta}_1 - l_{\mathrm{g}}\dot{\theta}_3\right)^2 + \frac{1}{2}c_2\left(l_{\mathrm{g}}\dot{\theta}_3 - l_{\mathrm{d}}\dot{\theta}_2\right)^2 \\ & + \frac{1}{2}c_3\dot{\theta}_3^2 + \frac{1}{2}c_4\left(\dot{\Delta}_{\mathrm{fl}}^2 + \dot{\Delta}_{\mathrm{fr}}^2\right) + \frac{1}{2}c_5\left(\dot{\Delta}_{\mathrm{rl}}^2 + \dot{\Delta}_{\mathrm{rr}}^2\right) \\ & + fk_b l_{\mathrm{f}}\varphi_1 l_{\mathrm{b}}\dot{\theta}_1 + fk_b l_{\mathrm{f}}\varphi_2 l_{\mathrm{b}}\dot{\theta}_2, \end{aligned} \tag{4}$$

where c_{e} is the equivalent damping of front wheels around their kingpins; c_1 and c_2 are the damping of left and right steering tie rods, respectively; c_3 is the damping of pitman arm; c_4 and c_5 are the damping of front and rear suspensions, respectively; and f is the friction coefficient between the tires and the ground.

The generalized force in the system is expressed as

$$\begin{aligned} Q_i = {} & F_{Y1}\frac{\partial}{\partial\dot{q}_i}\left[-(R\gamma + e)\dot{\theta}_1 + R\dot{\varphi}_1\right] \\ & + F_{Y2}\frac{\partial}{\partial\dot{q}_i}\left[-(R\gamma + e)\dot{\theta}_2 + R\dot{\varphi}_2\right]. \end{aligned} \tag{5}$$

Each generalized force corresponding to the generalized coordinate in the system can be given by

$$\begin{aligned} Q_1 &= -F_{Y1}(R\gamma + e), \\ Q_2 &= -F_{Y2}(R\gamma + e), \\ Q_3 &= 0, \\ Q_4 &= F_{Y1}R, \\ Q_5 &= F_{Y2}R, \\ Q_6 &= 0, \\ Q_7 &= 0, \\ Q_8 &= 0, \\ Q_9 &= 0, \end{aligned} \tag{6}$$

where F_{Y1} and F_{Y2} are the lateral forces of front-left wheel and front-right wheel, respectively, and e is the pneumatic trail of tire.

The displacement caused by angle change of each DoF is nonlinear. To simplify the model and calculation, assume the angles in equations (2)–(6) are small; thus, equation $\sin\theta = \theta$ holds, where $\theta \in [\theta_1\ \theta_2\ \theta_3\ \varphi_1\ \varphi_2\ \theta_{\mathrm{r}}\ \theta_{\mathrm{p}}\ \theta_\omega]$.

2.3. Calculation of Suspension Deformation. The diagram used to calculate the deformation of vehicle suspensions when shimmy occurs is shown in Figure 2. Thus, the deformation of vehicle suspensions Δ_{fl}, Δ_{fr}, Δ_{rl}, and Δ_{rr} can be deduced by

$$\begin{aligned} \Delta_{\mathrm{fl}} &= l'_{\mathrm{sfl}} - l_{\mathrm{sfl}} = \sqrt{\left(l_{\mathrm{h}} - l_{\mathrm{ac}}\varphi_1 + W_{\mathrm{f}}\theta_{\mathrm{r}} - L_{\mathrm{f}}\theta_{\mathrm{p}} + z\right)^2 + \left[l_{\mathrm{c}} + m\sin\theta_{\mathrm{a}} - m\sin(\theta_{\mathrm{a}} + \theta_\omega)\right]^2 + \left[m\cos\theta_{\mathrm{a}} - m\cos(\theta_{\mathrm{a}} + \theta_\omega)\right]^2} - \sqrt{l_{\mathrm{h}}^2 + l_{\mathrm{c}}^2}, \\ \Delta_{\mathrm{fr}} &= l'_{\mathrm{sfr}} - l_{\mathrm{sfr}} = \sqrt{\left(l_{\mathrm{h}} + l_{\mathrm{ac}}\varphi_1 - W_{\mathrm{f}}\theta_{\mathrm{r}} - L_{\mathrm{f}}\theta_{\mathrm{p}} + z\right)^2 + \left[l_{\mathrm{c}} + m\sin\theta_{\mathrm{a}} - m\sin(\theta_{\mathrm{a}} - \theta_\omega)\right]^2 + \left[m\cos\theta_{\mathrm{a}} - m\cos(\theta_{\mathrm{a}} - \theta_\omega)\right]^2} - \sqrt{l_{\mathrm{h}}^2 + l_{\mathrm{c}}^2}, \\ \Delta_{\mathrm{rl}} &= l'_{\mathrm{srl}} - l_{\mathrm{srl}} = \sqrt{\left(l_{\mathrm{h}} + W_{\mathrm{r}}\theta_{\mathrm{r}} + L_{\mathrm{r}}\theta_{\mathrm{p}} + z\right)^2 + \left[n\sin\theta_{\mathrm{b}} - n\sin(\theta_{\mathrm{b}} - \theta_\omega)\right]^2 + \left[n\cos\theta_{\mathrm{b}} - n\cos(\theta_{\mathrm{b}} - \theta_\omega)\right]^2} - l_{\mathrm{h}}, \\ \Delta_{\mathrm{rr}} &= l'_{\mathrm{srr}} - l_{\mathrm{srr}} = \sqrt{\left(l_{\mathrm{h}} - W_{\mathrm{r}}\theta_{\mathrm{r}} + L_{\mathrm{r}}\theta_{\mathrm{p}} + z\right)^2 + \left[n\ \sin\theta_{\mathrm{b}} - n\sin(\theta_{\mathrm{b}} + \theta_\omega)\right]^2 + \left[n\cos\theta_{\mathrm{b}} - n\cos(\theta_{\mathrm{b}} + \theta_\omega)\right]^2} - l_{\mathrm{h}}, \end{aligned} \tag{7}$$

where l_{sfl}, l_{sfr}, l_{srl}, and l_{srr} are the original lengths of front-left, front-right, rear-left, and rear-right suspension springs; l'_{sfl}, l'_{sfr}, l'_{sfl}, and l'_{srr} are the lengths of springs after deformation corresponding to l_{sfl}, l_{sfr}, l_{srl}, and l_{srr}; m and n are the distances from vehicle body's CoG to the connection points between front suspensions and vehicle body and between rear suspensions and vehicle body; θ_{a} and θ_{b} are the angles between line m and x axis and between line n and x axis; θ_{s} is the inclination angle of front suspension, which is defined as the angle between the central line of spring in front suspension and the horizontal plane; and make $l_{\mathrm{ac}} = l_{\mathrm{a}} + l_{\mathrm{c}}$. These parameters are all marked on Figure 2.

It can be seen clearly from equation (7) that the deformation of suspensions is nonlinear. Based on the above small angle change hypothesis, the linearized formulas for calculating the deformation of four vehicle suspensions when shimmy occurs are given as

$$\begin{aligned} \Delta_{\mathrm{fl}} &= -k_{\mathrm{hc}}l_{\mathrm{ac}}\varphi_1 + k_{\mathrm{hc}}W_{\mathrm{f}}\theta_{\mathrm{r}} - k_{\mathrm{hc}}L_{\mathrm{f}}\theta_{\mathrm{p}} - k_{\mathrm{cc}}m\cos\theta_{\mathrm{a}}\theta_\omega + k_{\mathrm{hc}}z, \\ \Delta_{\mathrm{fr}} &= k_{\mathrm{hc}}l_{\mathrm{ac}}\varphi_2 - k_{\mathrm{hc}}W_{\mathrm{f}}\theta_{\mathrm{r}} - k_{\mathrm{hc}}L_{\mathrm{f}}\theta_{\mathrm{p}} + k_{\mathrm{cc}}m\cos\theta_{\mathrm{a}}\theta_\omega + k_{\mathrm{hc}}z, \\ \Delta_{\mathrm{rl}} &= W_{\mathrm{r}}\theta_{\mathrm{r}} + L_{\mathrm{r}}\theta_{\mathrm{p}} + z, \\ \Delta_{\mathrm{rr}} &= -W_{\mathrm{r}}\theta_{\mathrm{r}} + L_{\mathrm{r}}\theta_{\mathrm{p}} + z, \end{aligned} \tag{8}$$

where, k_{hc} and k_{cc} can be given by

$$\begin{aligned} k_{\mathrm{hc}} &= \frac{l_{\mathrm{h}}}{\sqrt{l_{\mathrm{h}}^2 + l_{\mathrm{c}}^2}}, \\ k_{\mathrm{cc}} &= \frac{l_{\mathrm{c}}}{\sqrt{l_{\mathrm{h}}^2 + l_{\mathrm{c}}^2}}. \end{aligned} \tag{9}$$

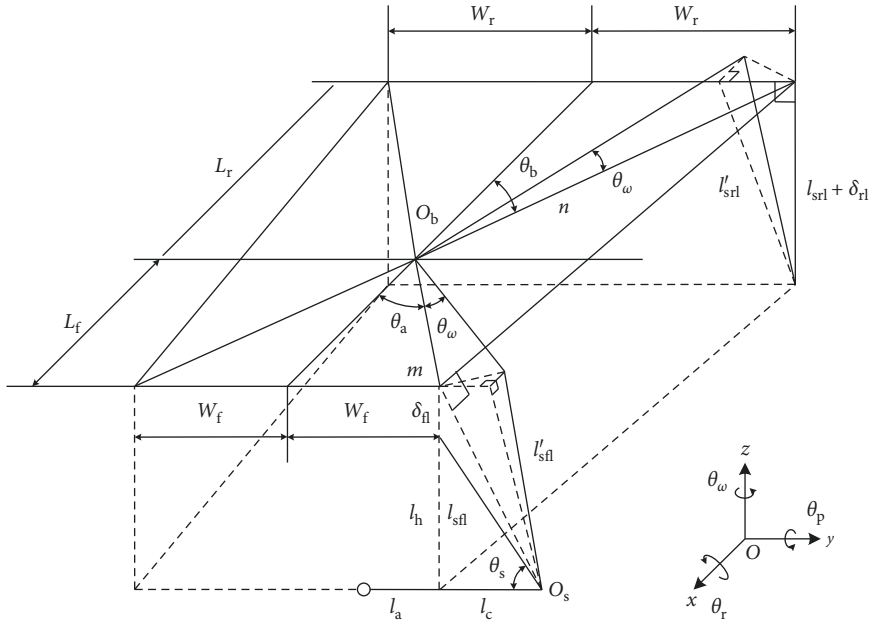

Figure 2: Diagram for calculating the deformation of front and rear suspensions when vehicle shimmy occurs.

2.4. Mathematical Model of Vehicle Shimmy with Consideration of the Motions of Vehicle Body. Based on the above analysis, the 9-DoF mathematical model of shimmy with consideration of the coupling effects of the motions of the vehicle body for a vehicle with double-wishbone independent front suspensions can be available, which is listed in equation (13).

In equation (13), the equivalent moment of inertia J_α, J_β, and J_γ are given by

$$\begin{aligned} J_\alpha &= \left(J_d + m_w l_b^2 + m_w l_b^2 \gamma^2\right), \\ J_\beta &= \left(J_d + J_d \gamma^2 + m_w l_f^2\right), \\ J_\gamma &= \left(J_d + m_w l_b l_f\right)\gamma. \end{aligned} \tag{10}$$

The seventh and the eighth terms of the first formula in equation (13) are caused by the lateral swing angle of front-left wheel axis φ_1, and they are torques acting on shimmy angle θ_1. Because the wheel rotates around its spin axis, when the wheel axis revolves around another axis, it is similar to a high-speed gyroscope rotating around its spin axis. Thus, the seventh term is the coupling torque caused by the elastic characteristics of the tire k_y and k_b, and the eighth term is the gyroscopic moment generated by the rotation of front-left wheel. It shows that there is coupling effect between the shimmy of front-left wheel around its kingpin and the lateral swing of front-left wheel axis around its lateral swing center. The same coupling effect also exists in the shimmy of front-right wheel and the lateral swing of front-right wheel axis.

The above conclusions can also be inferred from the first, second, fourth, and fifth formulas in equation (13), and another conclusion can be drawn from the sixth to the ninth formula in equation (13) that there are coupling effects between the motions of the vehicle body $\theta_{r,p,\omega}$ and z, and the motion of front wheel axes' lateral swing $\varphi_{1,2}$. Therefore, there are coupling effects between the shimmy of the front wheels and the motions of the vehicle body, and these coupling effects will be studied later.

2.5. Mathematical Model of Vehicle Shimmy Ignoring the Motions of Vehicle Body. Ignoring the coupling effects of the motions of vehicle body on shimmy, it can be assumed that the body is fixed. Thus, there is no displacement in each DoF of the vehicle body, that is to say, equations $\theta_r = 0$, $\theta_p = 0$, $\theta_\omega = 0$, and $z = 0$ hold. Substituting them into equation (13), the 5-DoF mathematical model of shimmy, including the angles of front wheels' shimmy $\theta_{1,2}$, the angle of pitman arm's swing θ_3, and the angles of front wheel axes' lateral swing $\varphi_{1,2}$, can be obtained, and its differential equation is listed in equation (14).

2.6. Tire Model and Tire Rolling Constraint Equation. Vehicle self-excited shimmy is a nonlinear dynamic bifurcation phenomenon, and it is one of the key factors that precisely expresses the cornering characteristics of the tire to accurately and effectively analyze the shimmy of the front wheels. As mentioned above, the nonlinear tire models that are commonly used in the simulation of vehicle dynamics mainly include Gim's tire models, Pacejka's Magic Formula, and Guokonghui's semiempirical tire theoretical model. The Magic Formula was chosen as the tire model in this study [19], and the lateral force of the tire can be given as

$$\begin{aligned} F_Y = D \sin\{C \arctan[B(\alpha - S_H)(1 - E) \\ + E \arctan B(\alpha - S_H)]\} + S_V, \end{aligned} \tag{11}$$

where α is the side-slip angle of wheel, B is the stiffness factor, C is the shape factor, D is the peak value, E is the

curvature factor, S_H is the horizontal shift, and S_V is the vertical shift, respectively. Here, we take $S_H = 0$ and $S_V = 0$, and B, C, D, E can be solved by

$$\begin{aligned} C &= a_0, \\ D &= a_1 F_z^2 + a_2 F_z, \\ BCD &= a_3 \sin\left(2 \arctan \frac{F_z}{a_4}\right) \times (1 - a_5|\beta|), \\ E &= a_6 F_z + a_7, \end{aligned} \tag{12}$$

$$\begin{aligned}
&J_\alpha \ddot{\theta}_1 - J_\gamma \ddot{\varphi}_1 + \left(k_1 l_d^2 + k_y R^2 \gamma^2 + k_b l_b^2 \gamma^2\right)\theta_1 + \left(c_e + c_1 l_d^2\right)\dot{\theta}_1 \\
&\quad - k_1 l_d l_g \theta_3 - c_1 l_d l_g \dot{\theta}_3 - \left[k_y R^2 \gamma + k_b l_b l_f (\gamma - f)\right]\varphi_1 \\
&\quad + J_0 \frac{v}{R} \dot{\varphi}_1 = F_{Y1}(R\gamma + e), \\
&J_\alpha \ddot{\theta}_2 - J_\gamma \ddot{\varphi}_2 + \left(k_2 l_d^2 + k_y R^2 \gamma^2 + k_b l_b^2 \gamma^2\right)\theta_2 + \left(c_e + c_2 l_d^2\right)\dot{\theta}_2 \\
&\quad - k_2 l_d l_g \theta_3 - c_2 l_d l_g \dot{\theta}_3 - \left[k_y R^2 \gamma + k_b l_b l_f (\gamma - f)\right]\varphi_2 \\
&\quad + J_0 \frac{v}{R} \dot{\varphi}_2 = F_{Y2}(R\gamma + e), \\
&J_3 \ddot{\theta}_3 - k_1 l_d l_g \theta_1 - c_1 l_d l_g \dot{\theta}_1 - k_2 l_d l_g \theta_2 - c_2 l_d l_g \dot{\theta}_2 \\
&\quad + \left(k_1 l_g^2 + k_2 l_g^2 + k_3\right)\theta_3 + \left(c_1 l_g^2 + c_4 l_g^2 + c_5\right)\dot{\theta}_3 = 0, \\
&J_\beta \ddot{\varphi}_1 - J_\gamma \ddot{\theta}_1 - \left(k_y R^2 + k_b l_b l_f\right)\gamma\theta_1 - J_0 \frac{v}{R}\dot{\theta}_1 \\
&\quad + \left(k_4 k_{hc}^2 l_{ac}^2 + k_y R^2 + k_b l_f^2\right)\varphi_1 + c_4 k_{hc}^2 l_{ac}^2 \dot{\varphi}_1 \\
&\quad - k_4 k_{hc}^2 l_{ac} W_f \theta_r - c_4 k_{hc}^2 l_{ac} W_f \dot{\theta}_r + k_4 k_{hc}^2 l_{ac} L_f \theta_p \\
&\quad + c_4 k_{hc}^2 l_{ac} L_f \dot{\theta}_p + k_4 k_{hc} k_{cc} l_{ac} m \cos\theta_a \theta_\omega \\
&\quad + c_4 k_{hc} k_{cc} l_{ac} m \cos\theta_a \dot{\theta}_\omega - k_4 k_{hc}^2 l_{ac} z \\
&\quad - c_4 k_{hc}^2 l_{ac} \dot{z} = -F_{Y1} R, \\
&J_\beta \ddot{\varphi}_2 - J_\gamma \ddot{\theta}_2 - \left(k_y R^2 + k_b l_b l_f\right)\gamma\theta_2 - J_0 \frac{v}{R}\dot{\theta}_2 \\
&\quad + \left(k_4 k_{hc}^2 l_{ac}^2 + k_y R^2 + k_b l_f^2\right)\varphi_2 + c_4 k_{hc}^2 l_{ac}^2 \dot{\varphi}_2 \\
&\quad - k_4 k_{hc}^2 l_{ac} W_f \theta_r - c_4 k_{hc}^2 l_{ac} W_f \dot{\theta}_r - k_4 k_{hc}^2 l_{ac} L_f \theta_p \\
&\quad - c_4 k_{hc}^2 l_{ac} L_f \dot{\theta}_p + k_4 k_{hc} k_{cc} l_{ac} m \cos\theta_a \theta_\omega \\
&\quad + c_4 k_{hc} k_{cc} l_{ac} m \cos\theta_a \dot{\theta}_\omega + k_4 k_{hc}^2 l_{ac} z \\
&\quad + c_4 k_{hc}^2 l_{ac} \dot{z} = -F_{Y2} R, \\
&J_r \ddot{\theta}_r - k_4 k_{hc}^2 l_{ac} W_f \varphi_1 - c_4 k_{hc}^2 l_{ac} W_f \dot{\varphi}_1 - k_4 k_{hc}^2 l_{ac} W_f \varphi_2 \\
&\quad - c_4 k_{hc}^2 l_{ac} W_f \dot{\varphi}_2 + 2\left(k_4 k_{hc}^2 W_f^2 + k_5 W_r^2\right)\theta_r \\
&\quad + 2\left(c_4 k_{hc}^2 W_f^2 + c_5 W_r^2\right)\dot{\theta}_r - 2k_4 k_{hc} k_{cc} W_f m \cos\theta_a \theta_\omega \\
&\quad - 2c_4 k_{hc} k_{cc} W_f m \cos\theta_a \dot{\theta}_\omega = 0, \\
&J_p \ddot{\theta}_p + k_4 k_{hc}^2 l_{ac} L_f \varphi_1 + c_4 k_{hc}^2 l_{ac} L_f \dot{\varphi}_1 - k_4 k_{hc}^2 l_{ac} L_f \varphi_2 \\
&\quad - c_4 k_{hc}^2 l_{ac} L_f \dot{\varphi}_2 + 2\left(k_4 k_{hc}^2 L_f^2 + k_5 L_r^2\right)\theta_p \\
&\quad + 2\left(c_4 k_{hc}^2 L_f^2 + c_5 L_r^2\right)\dot{\theta}_p - 2\left(k_4 k_{hc}^2 L_f - k_5 L_r\right)z \\
&\quad - 2\left(c_4 k_{hc}^2 L_f - c_5 L_r\right)\dot{z} = 0,
\end{aligned}$$

$$\begin{aligned}
&J_\omega \ddot{\theta}_\omega + k_4 k_{cc} k_{hc} l_{ac} m \cos\theta_a \varphi_1 + c_4 k_{cc} k_{hc} l_{ac} m \cos\theta_a \dot{\varphi}_1 \\
&\quad + k_4 k_{hc} k_{cc} l_{ac} m \cos\theta_a \varphi_2 + c_4 k_{hc} k_{cc} l_{ac} m \cos\theta_a \dot{\varphi}_2 \\
&\quad - 2k_4 k_{hc} k_{cc} W_f m \cos\theta_a \theta_r - 2c_4 k_{hc} k_{cc} W_f m \cos\theta_a \dot{\theta}_r \\
&\quad + 2k_4 k_{cc}^2 m^2 \cos^2\theta_a \theta_\omega + 2c_4 k_{cc}^2 m^2 \cos^2\theta_a \dot{\theta}_\omega = 0, \\
&m_s \ddot{z} - k_4 k_{hc}^2 l_{ac} \varphi_1 - c_4 k_{hc}^2 l_{ac} \dot{\varphi}_1 + k_4 k_{hc}^2 l_{ac} \varphi_2 \\
&\quad + c_4 k_{hc}^2 l_{ac} \dot{\varphi}_2 - 2\left(k_4 k_{hc}^2 L_f - k_5 L_r\right)\theta_p - 2\left(c_4 k_{hc}^2 L_f - c_5 L_r\right)\dot{\theta}_p \\
&\quad + 2\left(k_4 k_{hc}^2 + k_5\right)z + 2\left(c_4 k_{hc}^2 + c_5\right)\dot{z} = 0,
\end{aligned} \tag{13}$$

$$\begin{aligned}
&J_\alpha \ddot{\theta}_1 - J_\gamma \ddot{\varphi}_1 + \left(k_1 l_d^2 + k_y R^2 \gamma^2 + k_b l_b^2 \gamma^2\right)\theta_1 + \left(c_e + c_1 l_d^2\right)\dot{\theta}_1 \\
&\quad - k_1 l_d l_g \theta_3 - c_1 l_d l_g \dot{\theta}_3 - \left[k_y R^2 \gamma + k_b l_b l_f (\gamma - f)\right]\varphi_1 + J_0 \frac{v}{R}\dot{\varphi}_1 \\
&\quad = F_{Y1}(R\gamma + e), \\
&J_\alpha \ddot{\theta}_2 - J_\gamma \ddot{\varphi}_2 + \left(k_2 l_d^2 + k_y R^2 \gamma^2 + k_b l_b^2 \gamma^2\right)\theta_2 \\
&\quad + \left(c_e + c_2 l_d^2\right)\dot{\theta}_2 - k_2 l_d l_g \theta_3 - c_2 l_d l_g \dot{\theta}_3 \\
&\quad - \left[k_y R^2 \gamma + k_b l_b l_f (\gamma - f)\right]\varphi_2 + J_0 \frac{v}{R}\dot{\varphi}_2 = F_{Y2}(R\gamma + e), \\
&J_3 \ddot{\theta}_3 - k_1 l_d l_g \theta_1 - c_1 l_d l_g \dot{\theta}_1 - k_2 l_d l_g \theta_2 - c_2 l_d l_g \dot{\theta}_2 \\
&\quad + \left(k_1 l_g^2 + k_2 l_g^2 + k_3\right)\theta_3 + \left(c_1 l_g^2 + c_4 l_g^2 + c_5\right)\dot{\theta}_3 = 0, \\
&J_\beta \ddot{\varphi}_1 - J_\gamma \ddot{\theta}_1 - \left(k_y R^2 + k_b l_b l_f\right)\gamma\theta_1 - J_0 \frac{v}{R}\dot{\theta}_1 \\
&\quad + \left(k_4 k_{hc}^2 l_{ac}^2 + k_y R^2 + k_b l_f^2\right)\varphi_1 + c_4 k_{hc}^2 l_{ac}^2 \dot{\varphi}_1 = -F_{Y1} R, \\
&J_\beta \ddot{\varphi}_2 - J_\gamma \ddot{\theta}_2 - \left(k_y R^2 + k_b l_b l_f\right)\gamma\theta_2 - J_0 \frac{v}{R}\dot{\theta}_2 \\
&\quad + \left(k_4 k_{hc}^2 l_{ac}^2 + k_y R^2 + k_b l_f^2\right)\varphi_2 + c_4 k_{hc}^2 l_{ac}^2 \dot{\varphi}_2 = -F_{Y2} R,
\end{aligned} \tag{14}$$

where F_z is the normal load acting on wheels, β is the camber angle of wheel, and the parameters $a_0, a_1, \ldots, a_7$ are all constants that have to be determined for each tire. In this study, the value of β is 0, and the values of $a_0, a_1, \ldots, a_7$ are listed in Table 1 (for choice of parameters, see Pacejka et al. [8, 19]).

It is assumed that the vehicle has no lateral acceleration; the normal load acting on the left wheel F_{z1} and the normal load acting on the right wheel F_{z2} are given as

$$\begin{aligned} F_{z1} &= F_{z0} - k_b l_f \varphi_1, \\ F_{z2} &= F_{z0} + k_b l_f \varphi_2, \end{aligned} \tag{15}$$

where F_{z0} is the static normal load acting on front-left and front-right wheels, which is given by

$$F_{z0} = \frac{1}{2} \frac{L_r'}{L_f' + L_r'} (m_s + 4m_w) g, \tag{16}$$

where L_f' and L_r' are the distances from the CoG of the vehicle to its front axle and rear axle, respectively.

The constraint of the side-slip angle and the shimmy angle of front wheel can be given as

Table 1: Values of the coefficients of Magic Formula.

Parameter	Value
a_0	1.65000
a_1	1250.00
a_2	12.80
a_3	−0.02103
a_4	−34.0
a_5	3036.00
a_6	0.00501
a_7	0.77394

$$\begin{aligned}\dot{\alpha}_1 + \frac{v}{\sigma}\alpha_1 + \frac{v}{\sigma}\theta_1 - \frac{a}{\sigma}\dot{\theta}_1 = 0,\\ \dot{\alpha}_2 + \frac{v}{\sigma}\alpha_2 + \frac{v}{\sigma}\theta_2 - \frac{a}{\sigma}\dot{\theta}_2 = 0,\end{aligned} \tag{17}$$

where σ is the relaxation length of tires and a is the half-length of the tire contact area. In this study, σ is 0.65 m and a is 0.2 m.

3. Existence Analysis of Hopf Bifurcation

According to equations (10)–(13) and equations (15)–(17), the state equation of the 9-DoF system with consideration of the motions of the vehicle body can be written as follows:

$$\dot{\mathbf{x}} = f(\boldsymbol{\delta}, v, \mathbf{x}), \tag{18}$$

where $\mathbf{x} \in R$ [19] is the state vector of the 9-DoF system and $\boldsymbol{\delta}$ is the parameter of the 9-DoF system. It is obvious that the system represented by equation (18) is a nonlinear autonomous system.

Making $\mathbf{x}_0 = 0 \in R$ [19] and substituting it into equation (13), the following equation can be derived.

$$\dot{\mathbf{x}}_i = f_i(\boldsymbol{\delta}, v, \mathbf{x}_0) = 0, \quad i = 1, 2, \ldots, 20. \tag{19}$$

Consequently, $\mathbf{x}_0$ is one of the equilibrium points of the system represented by equation (18).

When $\mathbf{x}$ varies in the vicinity of $\mathbf{x}_0$, the nonlinear differential equation (18) can be rewritten as following.

$$\dot{\mathbf{x}} = A(\boldsymbol{\delta}, v)\mathbf{x} + g(\boldsymbol{\delta}, v, \mathbf{x}). \tag{20}$$

In which, $A(\boldsymbol{\delta}, v)$ is the Jacobian matrix of equation (18) in the equilibrium point $\mathbf{x}_0$ and $g(\boldsymbol{\delta}, v, \mathbf{x})$ is the infinitesimal of higher order. Therefore, $A(\boldsymbol{\delta}, v)$ and $g(\boldsymbol{\delta}, v, \mathbf{x})$ are the linear part and the nonlinear part of equation (18), respectively.

The Jacobian matrix $A(\boldsymbol{\delta}, v)$ can be solved by

$$[A(\boldsymbol{\delta}, v)]_{i\times j} = \left.\frac{\partial f_i}{\partial x_j}\right|_{x=x_0}, \quad i, j = 1, 2, \ldots, 20. \tag{21}$$

The Jacobian matrix $A(\boldsymbol{\delta}, v)$ is a function of $\boldsymbol{\delta}$ and v; thus, if $\boldsymbol{\delta}$ and v are fixed, $A(\boldsymbol{\delta}, v)$ can be written as a constant matrix A.

In the same way, according to equations (10)–(12) and equations (14)–(17), the state equation of the 5-DoF system ignoring the motions of body can be written as the sum of linear part and nonlinear part, as follows:

$$\dot{\mathbf{x}}' = A'(\boldsymbol{\delta}', v)\mathbf{x}' + g'(\boldsymbol{\delta}', v, \mathbf{x}'). \tag{22}$$

In which, $\mathbf{x}' \in R$ [11] is the state vector of the 5-DoF system; $\boldsymbol{\delta}'$ is the parameters of 5-DoF system; $A'(\boldsymbol{\delta}', v)$ is the Jacobian matrix of 5-DoF system state equation in the equilibrium point $\mathbf{x}_0'$; and nonlinear part $g'(\boldsymbol{\delta}', v, \mathbf{x}')$ is the infinitesimal of higher order.

According to the nonlinear system theory, the Jacobian matrix of the nonlinear system in the equilibrium point can be used to analyze the stability of the system. It can be seen from equation (21) that the matrix A varies with velocity v; thus, the eigenvalues of the Jacobian matrix vary with vehicle velocity. For clearly illustrating the relationships between the eigenvalues of the Jacobian matrix and vehicle velocity, the eigenvalue loci of the Jacobian matrix A varying with vehicle velocity v are shown in Figure 3, and the eigenvalue loci of the Jacobian matrix A' of the 5-DoF system varying with vehicle velocity v are also drawn on.

It is obvious that the eigenvalue loci of the system are symmetrical on the real axis. The Jacobian matrix A of the 9-DoF system has 20 curves of eigenvalue locus, and the Jacobian matrix A' of the 5-DoF system has 12 curves of eigenvalue locus. With the increase of v from 0 m/s to 40 m/s, eight curves of eigenvalue locus of both systems vary obviously, among which, four eigenvalue loci pass through the imaginary axis from the left half of the complex plane to the right, and then come back to the left again, but the rest nearly have no change, which assemble into a point on the complex plane. The red points in the ellipse in Figure 3 are eigenvalue loci which relate to the vehicle body. It can be seen from Figure 3 that the eigenvalue loci of matrix A and A' have the same trend when vehicle velocity v increases, in addition to few differences.

Here, the Jacobian matrix A of the 9-DoF nonlinear system is used as an example to study the Hopf bifurcation characteristics of vehicle shimmy. The velocity at which the Jacobian matrix A has two conjugate purely imaginary eigenvalues, and the real parts of other eigenvalues are all negative, is called the critical velocity of the system. Figure 3 shows the system has two critical velocities v_1 and v_2 ($v_1 < v_2$). When $v < v_1$ or $v > v_2$, the real parts of all eigenvalues in matrix A are negative, and the system is stable asymptotically. When $v_1 < v < v_2$, matrix A has positive real part eigenvalues, and the original system has self-excited oscillation and produces limit cycles. When v varies at the vicinity of critical velocity, the eigenvalue loci of the Jacobian matrix A pass through the imaginary axis of the complex plane, so that the stability of vehicle shimmy changes. While vehicle velocity v increases or decreases to the critical velocity, that is, when the eigenvalue loci of the system pass through the imaginary axis, the nonlinear system (18) will produce the Hopf bifurcation, and the critical velocity is the bifurcation point. Thus, shimmy occurs only when the Jacobian matrix A of the system has positive real part eigenvalues, and it is obvious that vehicle shimmy occurs in the moderate velocity range. The 5-DoF system has the similar Hopf bifurcation characteristic as the 9-DoF system, and its Hopf bifurcation characteristic and stability can also be analyzed in the same way.

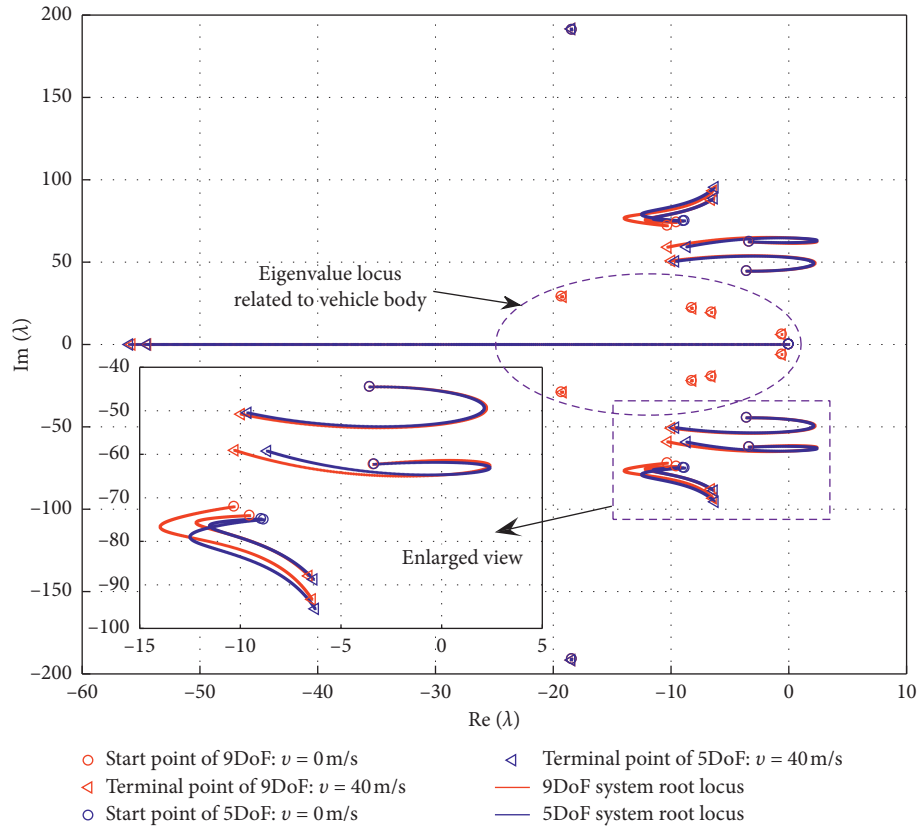

Figure 3: Eigenvalue loci of 9-DoF shimmy and 5-DoF shimmy.

4. Numerical Simulation

Based on the mathematic model of vehicle shimmy, the dynamic response of each DoF can be discussed by means of numerical simulation, and the coupling effects between the motions of the vehicle body and the shimmy of front wheels will be studied. It is assumed that a 0.01 rad angular displacement is exerted on the front-left wheel as initial excitation. Based on equations (10)–(17) and the parameters listed in Tables 1 and 2 (for choice of parameters in Table 2, see Wei et al. [14] and Mi et al. [18]), numerical simulation can be carried out. The dynamic responses of front wheels' shimmy, pitman arm's swing, and front wheel axes' lateral swing in two systems at the velocity of 10 m/s are shown as Figures 4–6, where the time history response and steady-state phase portrait of each DoF are drawn on. It is assumed that the time is $t = 0$ s when the initial excitation is exerted.

The dynamic responses of front wheels' shimmy and pitman arm's swing are shown in Figure 4. It shows that the shimmy of front wheels and the swing of pitman arm step into the steady state at about 3 s, and their steady-state phase portraits are definitely limit cycles. The amplitudes of front wheels' shimmy in the steady state are far beyond the initial excitation which is exerted on it.

The dynamic responses of front wheel axes' lateral swing are shown in Figure 5. Because of the coupling effects, the lateral swing of front wheel axes gradually steps into stable oscillation with the shimmy of the front wheels at the same time, but their phase portraits are not symmetrical. There are little deviations between the equilibrium positions of the lateral swing and their corresponding original positions, and their equilibrium positions are drawn on with a green line.

Due to the coupling effects, the body vibrates with the shimmy of the front wheels. The dynamic responses of the motions of the vehicle body are shown in Figure 6. The dynamic courses of the pitch and vertical motions of vehicle body show as violent vibrations. Similar to the lateral swing of front wheel axes, there are deviations between the equilibrium positions of the pitch and vertical motions and their corresponding original positions when the vehicle body vibrates, and their equilibrium positions are drawn on with a green line. Moreover, it can be seen from the sixth and the eighth formulas in equation (13) that there is coupling effect between the roll and yaw motions, and it also can be seen from the seventh and the ninth formulas in equation (13) that the coupling effect between pitch motion and vertical motion exists. Therefore, as shown in Figure 6, the roll motion has similar dynamic behavior as the yaw motion, and the pitch motion has similar dynamic behavior as the vertical motion.

Figures 4 and 5 show that the dynamic behavior of each DoF in the above two systems are similar, but the amplitude of each DoF in a 9-DoF system is bigger than that in a 5-DoF system when $v = 10$ m/s.

Table 2: Values of the parameters of vehicle shimmy.

Parameter	Value
J_0	8 (kg·m^2)
J_d	6 (kg·m^2)
J_3	3 (kg·m^2)
m_w	60 (kg)
m_s	1248 (kg)
J_r	325.52 (kg·m^2)
J_p	1229.82 (kg·m^2)
J_ω	1255.82 (kg·m^2)
L_f'	1.220 (m)
L_r'	1.473 (m)
L_f	1.220 (m)
L_r	1.473 (m)
W_f	0.370 (m)
W_r	0.440 (m)
k_1	2240 (kN·m^{-1})
k_2	2240 (kN·m^{-1})
k_3	60 (kN·m^{-1})
k_4	200 (kN·m^{-1})
k_5	220 (kN·m^{-1})
c_1	630 (N·s·m^{-1})
c_2	630 (N·s·m^{-1})
c_3	100 (N·s·m^{-1})
c_4	6560 (N·s·m^{-1})
c_5	7120 (N·s·m^{-1})
c_e	44 (N·s·m)
k_y	68 (kN·m^{-1})
k_b	360 (kN·m^{-1})
F	0.015
γ	0.06 (rad)
R	0.40 (m)
E	0.07 (m)
l_a	0.140 (m)
l_b	0.200 (m)
l_c	0.160 (m)
l_d	0.126 (m)
l_f	0.612 (m)
l_g	0.100 (m)
l_h	0.400 (m)

5. Influences of Vehicle Parameters on Vehicle Shimmy

The dynamic behavior of vehicle shimmy depends on vehicle parameters and velocity, thus the relationship between the amplitude of each DoF and vehicle velocity, the influences of vehicle parameters such as the mass of vehicle body, the longitudinal position of vehicle body's CoG and the inclination angle of front suspension on the amplitude of each DoF, and the influences of theses parameters on velocity range of shimmy are studied.

5.1. Relationship between the Amplitude of Each DoF and Vehicle Velocity. The relationship between the amplitude of each DoF in a 9-DoF system and a 5-DoF system and vehicle velocity is studied, and the results are shown in Figure 7. Conclusions can be drawn as follows:

(1) The curves around which the amplitudes of front wheels' shimmy and pitman arm's swing vary with vehicle velocity are arched, which is consistent with the conclusion in the study of Lu et al. [17] and Mi et al. [18].

(2) The curves around which the amplitudes of front wheel axes' lateral swing and the motions of the vehicle body vary with vehicle velocity present saddle shape whose local maximum is found in the high-velocity region and the low-velocity region, and the local minimum is found in the medium-velocity region.

(3) If vehicle velocity is in the medium-velocity region, the amplitudes of front wheels' shimmy and pitman arm's swing are relatively big, and the amplitudes of other DoFs are relatively small.

(4) The amplitude of each DoF in the 9-DoF system is bigger than that in the 5-DoF system in the low-velocity region and smaller in the high-velocity region.

(5) The critical velocities of the 9-DoF system are all smaller than those of the 5-DoF system, thus its velocity range of shimmy moves to the low-velocity region.

5.2. Influences of the Mass of Vehicle Body. Since the forces acting on suspensions and tires vary with m_s, the dynamic response of each DoF of vehicle shimmy is likely to be affected by it. So the influences of m_s on the amplitude of each DoF are studied when vehicle shimmies, and results are shown in Figure 8. Conclusions can be made as follows:

(1) If m_s is big enough, the amplitudes of front wheels' shimmy, pitman arm's swing and front wheel axes' lateral swing all increase with the increment of m_s, and the increments are obviously big.

(2) If m_s is relatively small, the amplitudes of the motions of vehicle body increase with the increment of m_s, But when m_s is relatively big, the influences of the increment of m_s on the amplitudes of the motions of vehicle body are not distinct.

(3) If m_s is small, the normal loads acting on front wheels are too small to produce enough torque acting on the kingpin to keep vehicle shimmy.

5.3. Influences of the Longitudinal Position of Vehicle Body's CoG. It is assumed that the CoG of the vehicle body coincides with the CoG of the whole vehicle, then equations $L_f = L_f'$ and $L_r = L_r'$ hold, and the ratio of L_f and L_r (L_f: L_r) corresponds to the longitudinal position of the vehicle body's CoG. When the vehicle body's CoG moves backward, L_f increases and L_r decreases, and the value of L_f: L_r increases. The influences of the longitudinal position of vehicle body's CoG on the amplitude of each DoF are studied when vehicle shimmies, and results are shown in Figure 9. When the vehicle body's CoG moves backward, conclusions can be drawn as follows:

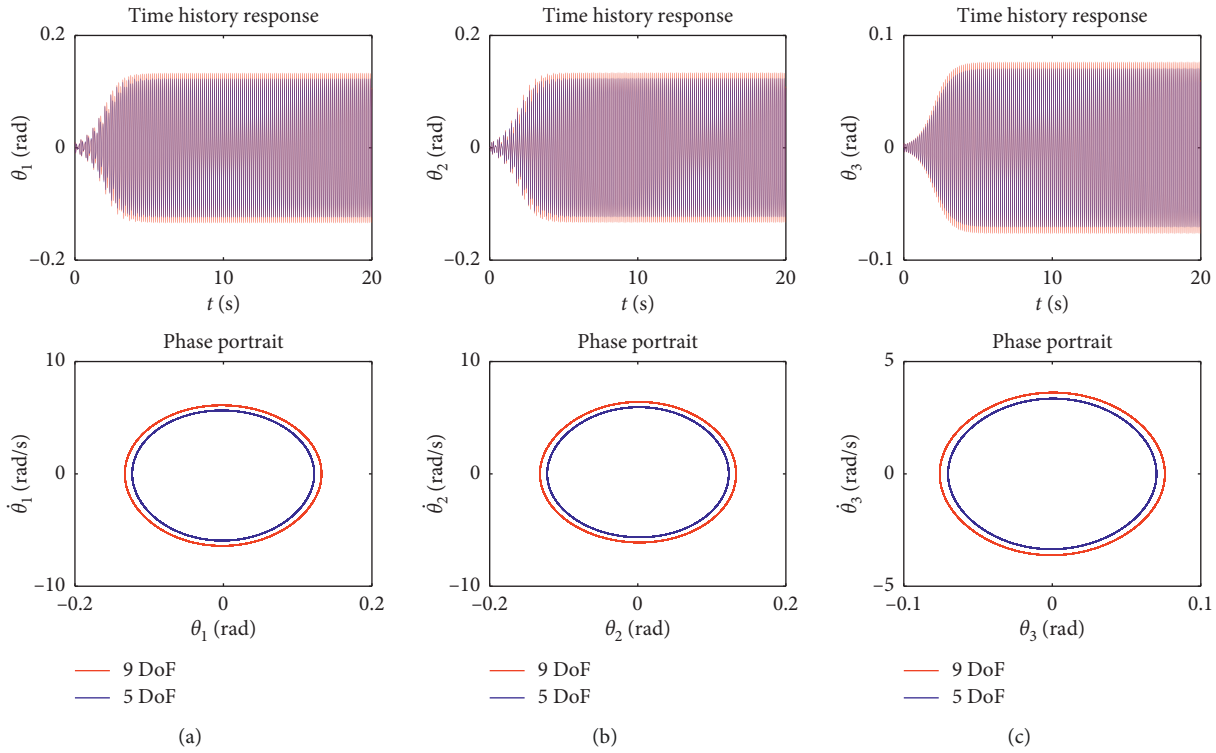

Figure 4: Dynamic responses of front wheels' shimmy and pitman arm's swing. (a) Front-left wheel. (b) Front-right wheel. (c) Pitman arm.

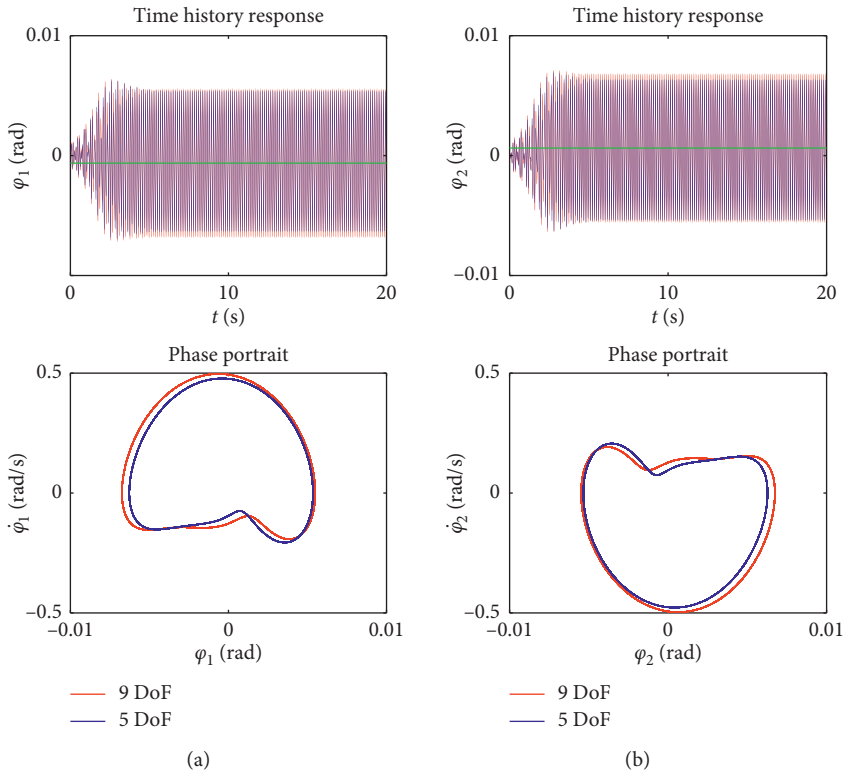

Figure 5: Dynamic responses of front wheel axes' lateral swing. (a) Front-left wheel axis. (b) Front-right wheel axis.

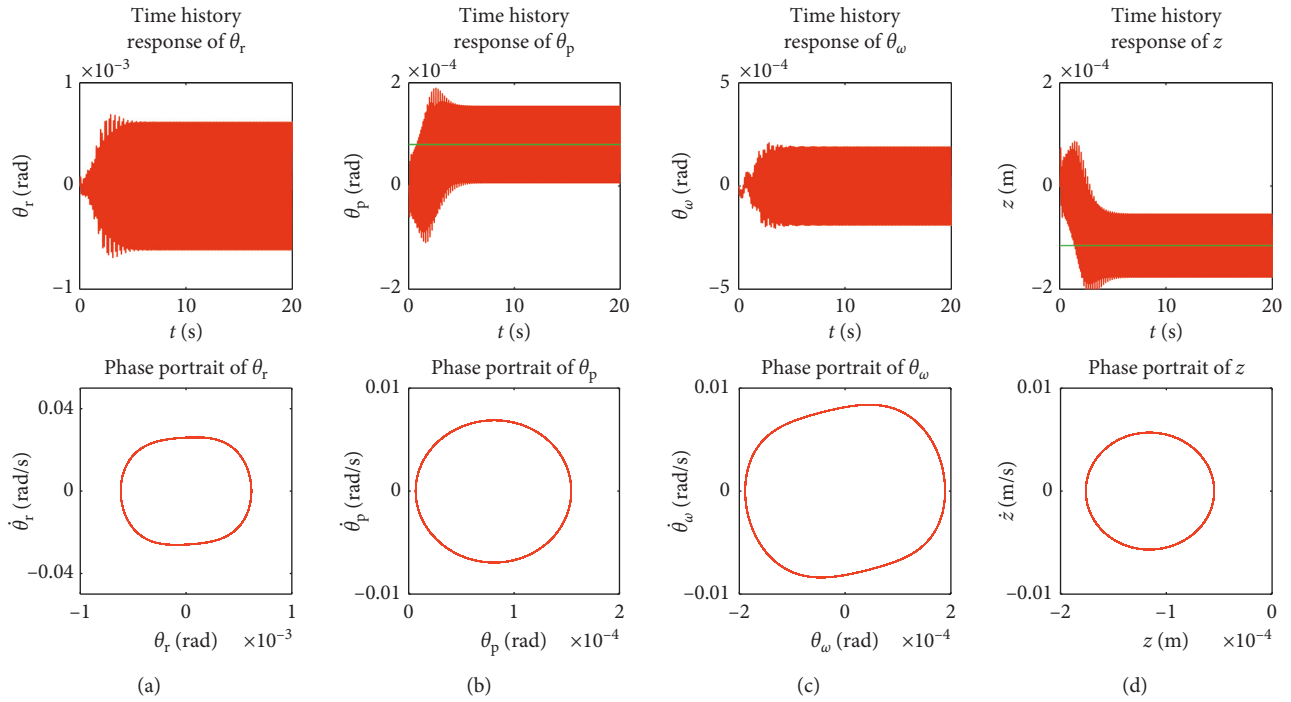

FIGURE 6: Dynamic responses of the motions of vehicle body. (a) Roll motion. (b) Pitch motion. (c) Yaw motion. (d) Vertical motion.

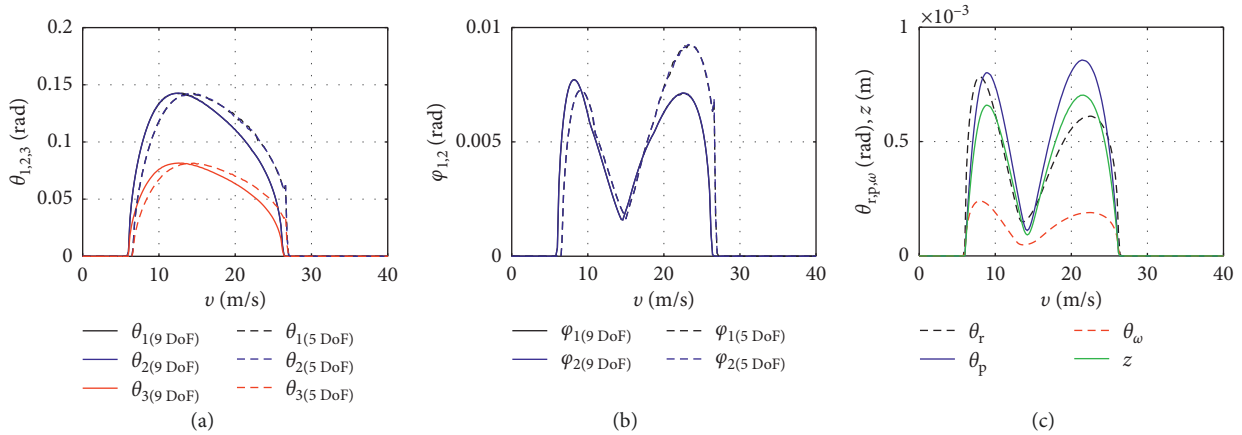

FIGURE 7: Relationship between the amplitude of each DoF and vehicle velocity. (a) The amplitudes of $\theta_{1,2,3}$. (b) The amplitudes of $\varphi_{1,2}$. (c) The amplitudes of $\theta_{r,p,\omega}$, and z.

(1) The amplitudes of front wheels' shimmy, pitman arm's swing, and front wheel axes' lateral swing all gradually decrease, and the decrement is relatively large.

(2) The amplitudes of the motions of the vehicle body gradually decrease. The decrement of the amplitudes of the roll motion and the vertical motion are relatively bigger, but the decrements of the amplitudes of the pitch motion and the yaw motion are relatively smaller.

(3) The normal load acting on the front wheels decreases. Thus, the torque acting on the kingpin decreases, and the amplitude of front wheels' shimmy decreases. Because of the coupling effects, the amplitudes of pitman arm's swing and front wheel axes' lateral swing and the motions of vehicle body decrease.

5.4. Influences of the Inclination Angles of Front Suspensions. The forces acting on the vehicle body and front suspensions vary with θ_s, so its influences on the amplitude of each DoF are studied when vehicle shimmies, and the results are shown in Figure 10. When θ_s increases, the following conclusions can be drawn:

(1) The amplitudes of front wheels' shimmy and pitman arm's swing all increase. But the increments of the amplitudes are small, and nearly cannot be seen.

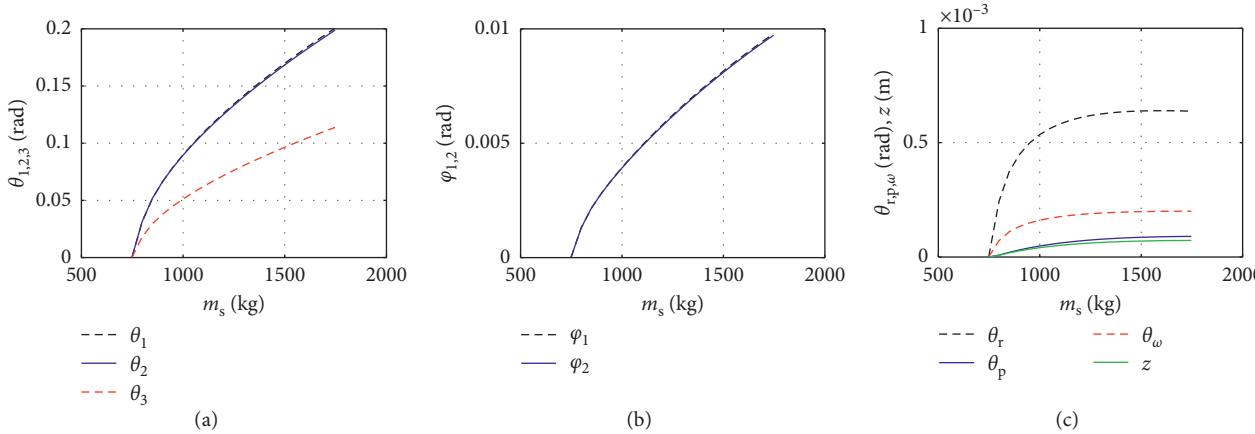

FIGURE 8: Influences of m_s on the amplitude of each DoF. (a) The amplitudes of $\theta_{1,2,3}$. (b) The amplitudes of $\varphi_{1,2}$. (c) The amplitudes of $\theta_{r,p,\omega}$, and z.

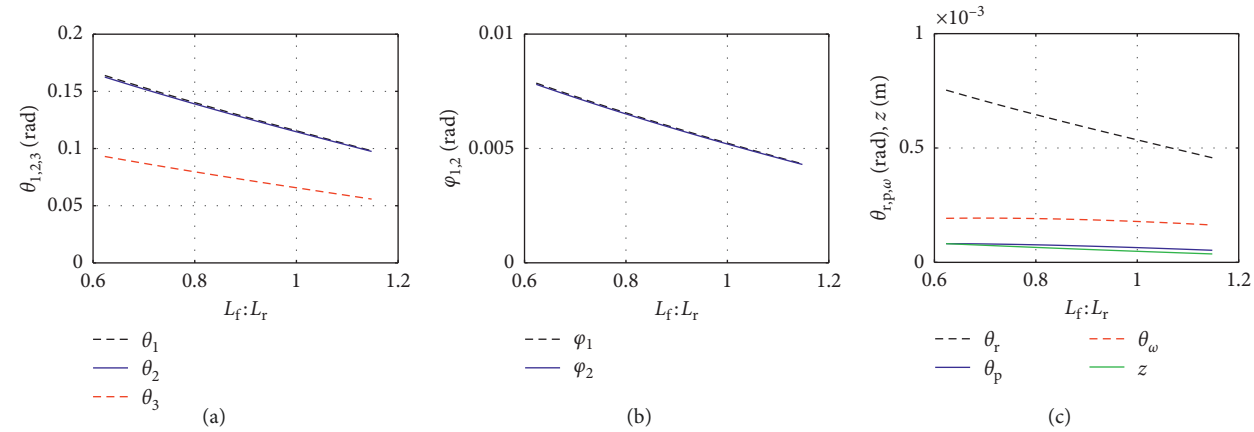

FIGURE 9: Influences of $L_f:L_r$ on the amplitude of each DoF. (a) The amplitudes of $\theta_{1,2,3}$. (b) The amplitudes of $\varphi_{1,2}$. (c) The amplitudes of $\theta_{r,p,\omega}$, and z.

(2) The amplitude of front wheel axes' lateral swing gradually decreases, but the decrement is small, and it is not obvious.

(3) The amplitudes of the roll motion, the pitch motion, and the vertical motion of the vehicle body increase, and the amplitude of the yaw motion of the vehicle body decreases to zero finally, but the increments of the pitch motion and the vertical motion are very small, and nearly cannot be seen.

(4) The normal forces acting on the front wheels have little changes, thus they have little influences on the amplitudes of front wheels' shimmy, pitman arm's swing, and front wheel axes' lateral swing.

(5) The vertical component force acting on vehicle body increases and the lateral component force decreases. Thus, the amplitude of pitch motion increases and the amplitude of the yaw motion decreases. But the amplitudes of the pitch motion and the vertical motion have little changes.

5.5. Influence on Velocity Range of Shimmy. As analyzed above, parameters such as m_s, the longitudinal position of vehicle body's CoG and θ_s influence the amplitude of each DoF of vehicle shimmy, thus the velocity range of shimmy must be influenced by these parameters. The influences of parameters on the velocity range of shimmy can be seen in Figure 11. Conclusions can be made as follows:

(1) The velocity range of shimmy will be enlarged with the increasing of m_s, in other words, if m_s increases, v_1 will decrease and v_2 will increase.

(2) The velocity range of shimmy will be narrowed if vehicle body's CoG moves back.

(3) The effect of θ_s on velocity range of shimmy is insignificant, and it nearly cannot be seen.

6. Conclusion

The coupling effects between the motions of the vehicle body and the shimmy of the front wheels are usually ignored in

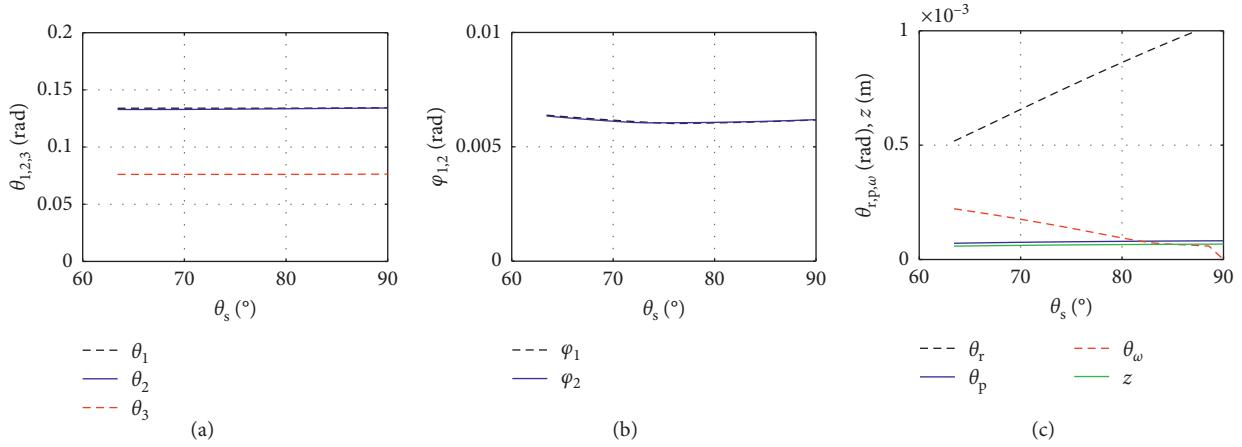

FIGURE 10: Influences of θ_s on the amplitude of each DoF. (a) The amplitudes of $\theta_{1,2,3}$. (b) The amplitudes of $\varphi_{1,2}$. (c) The amplitudes of $\theta_{r,p,\omega}$, and z.

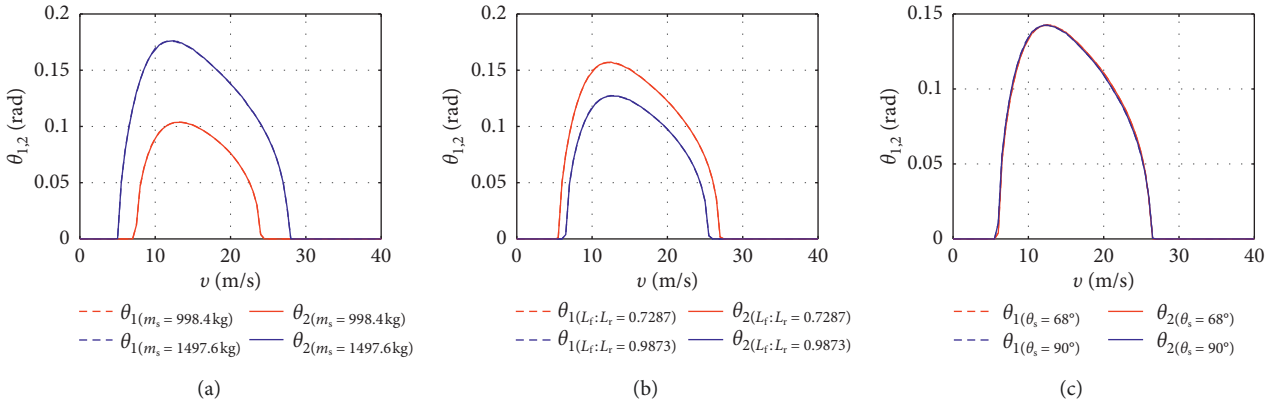

FIGURE 11: Influences of vehicle parameters on the critical velocity of vehicle shimmy. (a) Influences of m_s. (b) Influences of $L_f : L_r$. (c) Influences of θ_s.

previous research studies about vehicle shimmy. In this paper, a 9-DoF shimmy model of vehicle with consideration of the coupling effect of the motions of the vehicle body is established, and a 5-DoF shimmy model of vehicle ignoring these coupling effects is established according to the 9-DoF model. The dynamic behaviors of shimmy in two systems are compared. According to the above theoretical analyses and numerical simulation result, conclusions can be drawn as follows:

(1) If the effects of the motions of vehicle body on shimmy are take into account, the dynamic behaviors of front wheels, front wheel axes, and pitman arm are similar as that of ignoring the effects of the motions of the vehicle body, but the amplitude of each DoF in this system is bigger in low-velocity region and is smaller in high-velocity region.

(2) Because of the symmetry of vehicle mechanism, the shimmies of the front-left wheel and the front-right wheel and the lateral swings of the front-left wheel axis and the front-right wheel axis have the same dynamic performance.

(3) Because of the coupling effect, the roll motion and the yaw motion of vehicle body have similar dynamic behaviors, and the pitch motion and the vertical motion of vehicle body have similar dynamic behaviors.

(4) The amplitudes of the front wheels' shimmy and the motions of the vehicle body are all affected by the vehicle velocity.

(5) The mass of the vehicle body and the longitudinal position of the vehicle body's CoG have great influences on vehicle shimmy because they can change the normal forces acting on wheels.

(6) The inclination angle of front suspension has great influences on the roll motion and the yaw motion of vehicle body, but has little influences on other DoFs.

(7) Compared with the 5-DoF system, the velocity range of shimmy of the 9-DoF system moves to the low-velocity region, in other words, shimmy is more likely to occur in the low-speed region for a 9-DoF system.

(8) The mass of the vehicle body and the longitudinal position of vehicle body's CoG have obvious influences on velocity range of shimmy, but the inclination angle of front suspension has little influence.

Data Availability

All data generated or analyzed during this study are included in this published article.

Conflicts of Interest

The authors declare that they have no conflicts of interest.

Acknowledgments

The authors received the support of the National Natural Science Foundation of China (grant nos 51375086 and 51605087) and the Natural Science Foundation of Jiangsu Province, China (grant no. BK20160671). In the meantime, the authors would like to acknowledge the support of Dr. Tian Mi during this study.

References

[1] V. Cossalter, R. Lot, and F. Maggio, "The modal analysis of a motorcycle in straight running and on a curve," *Meccanica*, vol. 39, no. 1, pp. 1–16, 2004.

[2] M. A. Padmanabhan and E. H. Dowell, "Landing gear design/maintenance analysis for nonlinear shimmy," *Journal of Aircraft*, vol. 52, no. 5, pp. 1707–1710, 2015.

[3] C. Orlando and A. Alaimo, "A robust active control system for shimmy damping in the presence of free play and uncertainties," *Mechanical Systems and Signal Processing*, vol. 84, pp. 551–569, 2017.

[4] D. S. De Lavaud, "Shimmy, pseudo-shimmy and tramp of an automobile," *Comptes Rendus de l'Académie des Sciences de Paris*, vol. 185, pp. 254–257, 1927.

[5] B. Von Schlippe and R. Dietrich, "Das flattern eines bepneuten rades," *Bericht*, vol. 140, pp. 125–147, 1941.

[6] H. B. Pacejka, "Analysis of the shimmy phenomenon," *Proceedings of the Institution of Mechanical Engineers: Automobile Division*, vol. 180, no. 1, pp. 251–268, 1965.

[7] H. B. Pacejka, *The wheel shimmy phenomenon: a theoretical and experimental investigation with particular reference to the non-linear problem*, Ph.D. thesis, Delft University of Technology, Delft, Netherlands, 1966.

[8] E. Bakker, H. B. Pacejka, and L. Lidner, "A new tire model with an application in vehicle dynamics studies," 1989. SAE Technical Paper No. 890087.

[9] G. Gim and P. E. Nikravesh, "An analytical model of pneumatic tyres for vehicle dynamic simulations. Part 1: pure slips," *International Journal of Vehicle Design*, vol. 11, no. 6, pp. 589–618, 1990.

[10] K. Guo and D. Lu, "Unitire: unified tire model for vehicle dynamic simulation," *Vehicle System Dynamics*, vol. 45, no. 1, pp. 79–99, 2007.

[11] D. Takács and G. Stépan, "Experiments on quasi-periodic wheel shimmy," *Journal of Computational and Nonlinear Dynamics*, vol. 4, no. 3, pp. 983–990, 2009.

[12] D. Takács and G. Stépan, "Nonlinear oscillations at critical shimmy parameters: experiments and numerics," in *Proceedings of ASME 2010 International Mechanical Engineering Congress and Exposition*, pp. 731–739, Vancouver, BC, Canada, November 2010.

[13] S. Ran, I. J. M. Besselink, and H. Nijmeijer, "Energy analysis of the von schlippe tyre model with application to shimmy," *Vehicle System Dynamics*, vol. 53, no. 12, pp. 1795–1810, 2015.

[14] D. Wei, K. Xu, Y. Jiang, C. Chen, W. Zhao, and F. Zhou, "Hopf bifurcation characteristics of dual-front axle self-excited shimmy system for heavy truck considering dry friction," *Shock and Vibration*, vol. 2015, Article ID 839801, 20 pages, 2015.

[15] J.-W. Lu, J. Gu, and M.-J. Liu, "Modeling of the vehicle shimmy system with consideration of clearance of the steering linkage mechanism," *Meccanica*, vol. 45, no. 1, pp. 53–61, 2010.

[16] J. Lu, Y. Xu, C. Hu, A. F. Vakakis, and L. A. Bergman, "5-dof dynamic model of vehicle shimmy system with clearance at universal joint in steering handling mechanism," *Shock and Vibration*, vol. 20, no. 5, pp. 951–961, 2013.

[17] J.-W. Lu, J.-Y. Xin, A. F. Vakakis, and L. A. Bergman, "Influences of system parameters on dynamic behavior of the vehicle shimmy system with clearance in steering linkage," *Journal of Vibration and Control*, vol. 21, no. 2, pp. 359–370, 2015.

[18] T. Mi, G. Stepan, D. Takacs et al., "Shimmy model for electric vehicle with independent suspensions," *Proceedings of the Institution of Mechanical Engineers, Part D: Journal of Automobile Engineering*, vol. 232, no. 3, pp. 330–340, 2018.

[19] H. B. Pacejka, *Tire and Vehicle Dynamics*, Elsevier, Amsterdam, Netherlands, 3rd edition, 2012.